ASES SOLAR 2017
Building a 100% Renewable Energy Community
46th Annual National Solar Conference
AMERICAN SOLAR ENERGY SOCIETY | DENVER October 9-12

Conference Proceedings

ASES National Solar Conference 2017

Denver, Colorado 9-12 October 2017

Experimental Performance Testing and Thermal Modeling of an Integrated Solar Thermal Collector Energy Storage System

Kevin R. Anderson[1], Michael Yartzoff[1], Adam Chrisman[2], Nicholas Rocca[2]

[1] California State Polytechnic University, Pomona, CA (USA)

[2] SUNEARTH, Inc. Fontana, CA (USA)

Abstract

This paper presents the results of testing and modeling of an integrated solar thermal collector (STC) thermal energy storage (TES) system. These type of systems are often referred to as Integral Collector Storage (ICS) passive systems. The paper presents efficiency test data, f-chart analysis, and transient time analysis of a Sunearth, Inc. CP-20 ICS system. The paper explains the experiment test set up and efficiency curve determination and is followed by f-chart simulation and transient thermal modeling of the ICS. The data presented in this paper shows that the average efficiency of the system is η = 63% and the fraction of solar energy is on f= 32% for a scenario of hot water heating in the Southwest region of the USA.

Keywords: *Solar Thermal Collector, Thermal Energy Storage, Modeling, Testing*

1. Introduction

This paper presents testing and modeling for a passive Integral Collector Storage (ICS). The work by Smyth et al. (2004) provides an up to date review on the technology of ICS systems. Herein, the ICS considered in the Sunearth, Inc. CopperHeart Model CP-20 ICS which combines thermal collection and storage in a single unit. The device tested and modeled is shown in Figure 1.

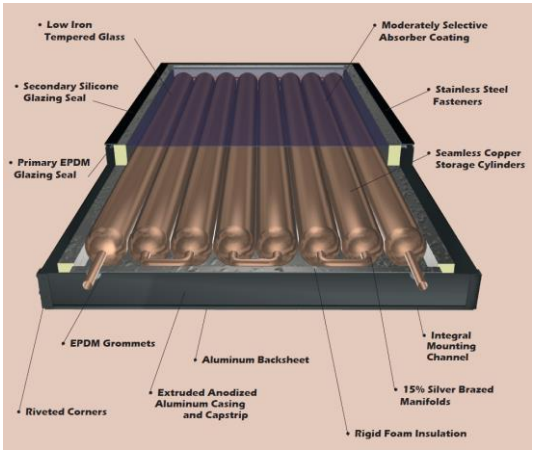

Fig. 1: Image of ICS system (cf. http://sunearthinc.com/)

The ICS is a solar thermal collector in which incident solar radiation is absorbed directly by the storage

medium (heat transfer working fluid). Thus, the physical operation of the ICS relies on the transfer of the solar energy from the collector to the heat transfer working fluid via natural convection, no outside energy is required, thus making it the ICS a completely passive system. While water is the typical working fluid, recently Kocaa et al. (2008) experimentally investigated the use of Phase Change Materials (PCM) in conjunction with the ICS. When hot water delivery is required, the solar heated water stored in the ICS flows out via the force of gravity or the pressure of the cold water replacing it and continues into the conventional backup water heating system inside the house. This type of hot water installation is considered to be a direct system (open-loop) since the water being heated is the same water that is being consumed for heating applications. The ICS (also called a "batch" or "breadbox" water heater) combines a solar collector and water storage tank into one single unit. The ICS can be easily added to an existing domestic hot water installations. However, there are a number of disadvantages with ICS systems such as weight, heat loss, efficiency and the possibility of freezing in cold weathers. In general, ICS units are more inefficient in cold climates, due to heat losses at night. The ICS systems are most suitable for mild and warmer climates, which prevents the stored water from freezing in winter. Since the collector doubles as a water storage device, some designs have double or triple glazing over the pipes or tanks to reduce heat loss. However, this adds to the overall weight and cost of the unit. While ICS systems depend on system demand for their flow, some models have been configured to use the thermosiphon principle. The thermosiphon ICS system uses the principle of natural convection of fluid between a collector and an elevated storage tank. As water is heated in the collector and it rises naturally to the tank above. The remaining part of this paper describes the experimental test set-up followed by an f-chart analysis and transient simulation of the ICS.

2. Experimental Set-up

In this section of the manuscript the experimental set-up is described followed by the determination of the efficiency curve of the ICS.

2.1. Experimental Test Configuration

The experimental apparatus is shown in Figure 2. The ICS unit was mounted to the roof of a storage container in Pomona, CA, USA. The installation was set an a constant inclinartion of 30 degrees tilt.

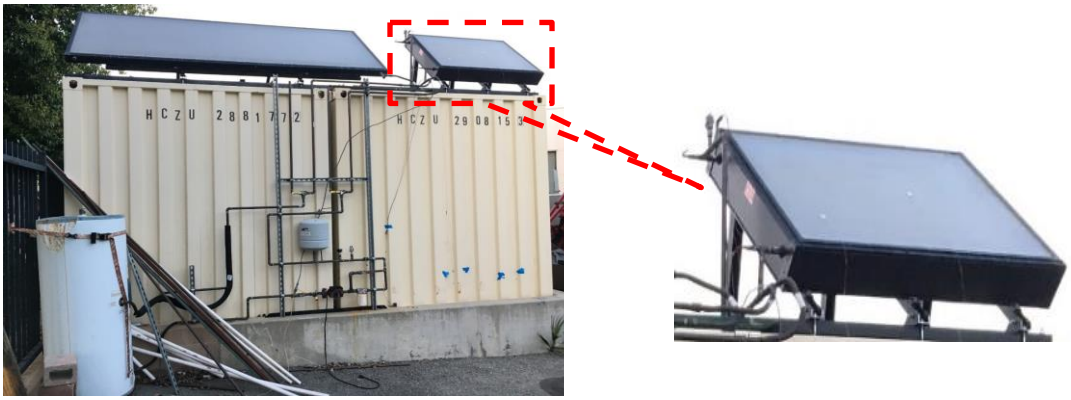

Fig. 2: Experimental test set-up for ICS system

The ICS unit was mounted on top of the storage container in the backyard of the engineering laboratory building at Cal Poly Pomona (CPP) and instrumented with one thermocouple mounted on the inlet water supply to the ICS, one thermocouple mounted to the exit water supply of the ICS, and two other thermocouples mounted on the glass covering. Additionally, a mass flow meter is used to record the flow rate of the water circulating in the system. A hand-held insolation meter is used to collect and record the daily average insolation values reach heat the system. The ICS tested has a capacity of 71.9228 Liters (19 US gallons), a collector area of 0.9195 m (36.2 inches) by 1.27508 m (50.2 inches) giving 1.172 m^2 (12.1 ft^2), and rated internal working pressure of 0.827 MPa (120 psi) at 93.3 °C (200 °F).

2.2. Efficiency Curve

The efficiency of the system is given by the following relationship per Goswami et al. (2000) and Struckmann (2008),

$$\eta = F_R\tau\alpha - F_R U_c\left(\frac{T_i - T_a}{I}\right) \qquad \text{(eq. 5)}$$

where the collector heat removal factor F_R is expressed as

$$F_R = \frac{\dot{m}C_p\left(T_o - T_i\right)}{A[I\tau\alpha - U_c(T_i - T_a)]} \qquad \text{(eq. 6)}$$

It is assumed that F_R, τ, α, U_c, are constants for a given collector and flow rate, then the efficiency is a linear function of the three remaining parameters defining the operating scenario: solar irradiance, *I*, fluid inlet temperature, T_i and ambient air temperature T_a as shown below

$$\eta = F_R\tau\alpha - F_R U_c\left(\frac{T_i - T_a}{I}\right) = b - m\frac{\Delta T}{I} \qquad \text{(eq. 7)}$$

where *b*= $F_R\tau\alpha$ and *m* = $F_R U_c$.

In Figure 6, the efficiency curve taken from the Solar Rating and Certification Corporation (SRCC) data sheet for the Sunearth CopperHeart CP-20 unit is plotted in comparison to the estimated efficiency curve tested at Cal Poly Pomona (CPP).

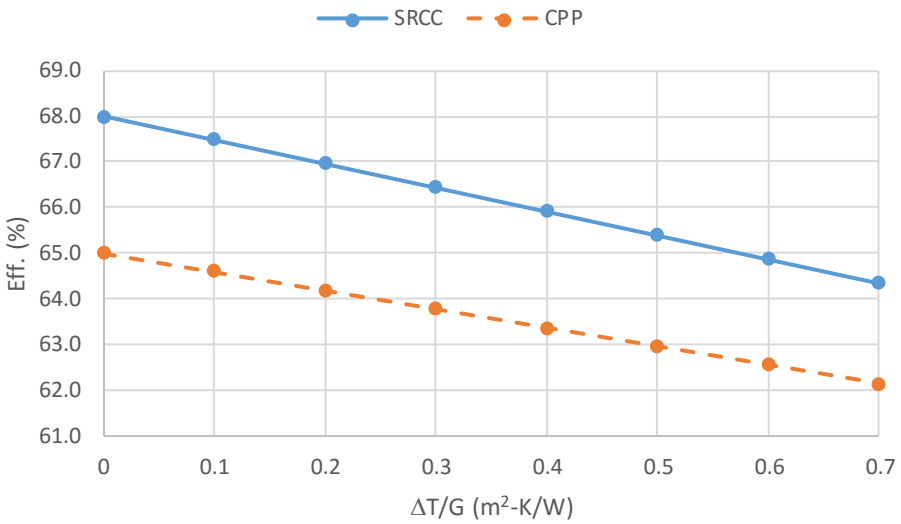

Fig. 6: Efficiency curve for ICS system

The test data sheet of SRCC gave *b* = 0.68 and *m* = 5.23 W/m^2-K in comparison to the CPP estimate of *b* = 0.65 and *m* = 4.1 W/m^2-K, taken from test data of the ICS. The percent error on the slope is thus found to be %error =100* |5.23-4.1|/5.23= 22%. The discrepancy in slope values from SRCC and CPP is believed to be due to installation effects and or instrumentation uncertainties at the CPP site (i.e. tree blockage as shown in Fig 1. and discrepancy in insolation values, and/or due to instrumentation mounting error, i.e. thermocouples on inlet / exit lines, not directly mounted on collector tubes). Further investigation is needed to address this. Nevertheless, the estimate of CPP slope of the ICS is conservative, owing to the fact that a rather constant efficiency value on average of 63% is predicted by the CPP value of slope and intercept of the ICS system.

2.3. F-chart Modelling

This section of the paper attempts to model the performance of the ICS. Preliminary modeling of ICS systems is documented in Tsilingiris (1996). Pioneering work in the simulation of ICS systems using f-chart can be found in Kalogirou (1999). A traditional f-chart analysis per Klein and Beckman (2008) was carried out on the ICS system. The f-chart method is a correlation of the results of a large number of thermal performance simulations of solar heating systems. The results give *f*, the fraction of the monthly heating load supplied by solar energy, as a function of the two dimensionless parameters i) *X*, the collector loss, and ii) *Y*, the collector gain. The collector loss is related to the ratio of collector losses to heating loads. The collector gain is related to the ratio of absorbed solar radiation to the heating loads. The f-chart analysis is based on the following suite of equations:

$$X = F_R U_c \frac{F'_R}{F_R}(T_{ref} - \overline{T}_a)\Delta\tau \frac{A_c}{L} \qquad \text{(eq. 10)}$$

$$Y = F_R\left(\tau\alpha\right)_n \frac{F'_R}{F_R}\frac{\left(\overline{\tau\alpha}\right)_n}{\left(\tau\alpha\right)_n}\overline{H}_T N \frac{A_c}{L} \qquad \text{(eq. 11)}$$

and for liquid systems such as the one at hand,

$$f = 1.029Y - 0.065X - 0.245Y^2 + 0.0018X^2 + 0.0215Y^3 \qquad \text{(eq. 12)}$$

with the fraction *F* of the annual heating load supplied by solar energy is the sum of the monthly solar energy contributions dived by the annual load:

$$F = \frac{\sum fL}{\sum L} \qquad \text{(eq. 14)}$$

The nomenclature of eq. 11 to eq. 14 is summarized in Klein at al. (1976) and Klein and Beckman (2008). Inputs to the f-chart analysis were a water volume / collector area ratio = 64 L/m^2 (1.57 gallons / ft^2), auxillary gas heating with 80% efficiency, daily hot water usage of 244.2 L (64.5 gallons), water temperature of 49 °C (120 °F), ambient temperature of 20 °C (68 °F), auxiliary storage tank thermal resistance value of R = 1/ UA = 0.471 K/W (0.249 hr-°F / BTU), pipe heat loss thermal resistance value of R = 1/ UA = 0.379 K/W (0.2 hr-°F / BTU)for both inlet and outlet, number of flat plate collectors = 1, collector panel area = 1.172 m^2 (12.1 ft^2), collector slope = 30°, collector flow rate / area = 0.02083 kg/s-m^2 (15.36 lb/hr-ft^2), collector working fluid specific heat = 4200 J/kg-K (1.0 BTU / lb-°F). Figure 9 shows the location input dialog of the f-chart demo version.

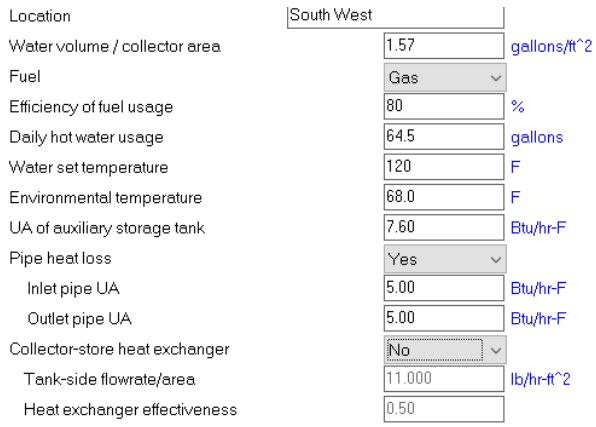

Fig. 9: F-chart program input

Figure 10 shows the user input dialog for the f-chart simulation of the ICS in using the SRCC reported slope / intercept data for the ICS.

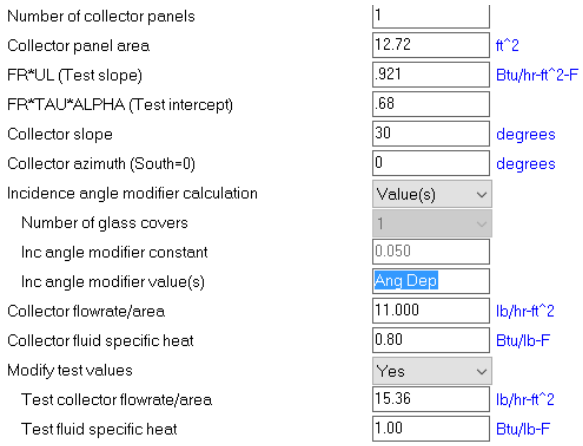

Fig. 10: F-chart input for ICS SRCC slope / intercept data

Figure 11 shows the user input dialog for the f-chart simulation of the ICS in using the CPP (Cal Poly Pomona) reported slope / intercept data for the ICS.

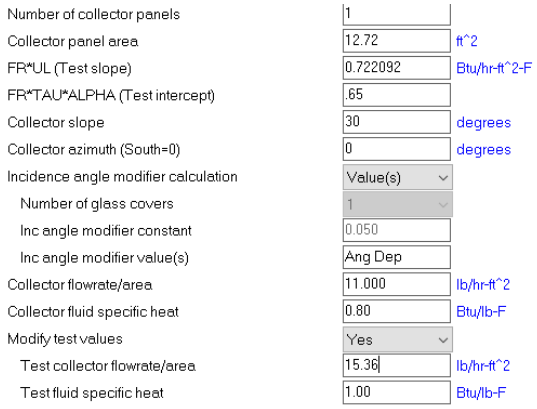

Fig. 11: F-chart input for ICS CPP slope / intercept data

Table 3 shows the output from the f-chart simulation using the SRCC input data.

Tab. 3: F-chart analysis summary SRCC

SRCC	Solar (10^6 BTU)	DHW (10^6 BTU)	AUX (10^6 BTU)	Solar (MJ)	DWH (MJ)	AUX (MJ)	f
Jan	0.585	1.14	1.012	617.2101	1202.768	1067.721	0.112
Feb	0.642	1.027	0.846	677.3485	1083.547	892.5808	0.176
Mar	0.827	1.132	0.867	872.5346	1194.328	914.737	0.234
Apr	0.929	1.089	0.756	980.1507	1148.96	797.6254	0.305
May	0.976	1.118	0.751	1029.739	1179.557	792.3501	0.329
Jun	0.932	1.076	0.713	983.3159	1135.245	752.2578	0.337
Jul	0.89	1.107	0.754	939.0034	1167.951	795.5152	0.319
Aug	0.891	1.108	0.76	940.0585	1169.006	801.8456	0.314
Sep	0.855	1.076	0.751	902.0763	1135.245	792.3501	0.302
Oct	0.796	1.122	0.848	839.8278	1183.777	894.6909	0.244
Nov	0.627	1.095	0.925	661.5226	1155.291	975.9305	0.156
Dec	0.548	1.138	1.029	578.1729	1200.658	1085.657	0.096
Year	9.499	13.229	10.014	10022.01	13957.39	10565.37	0.243

Table 4 shows the output from the f-chart simulation using the CPP input data.

Tab. 4: F-chart analysis summary CPP input data

CPP	Solar (10^6 BTU)	DHW (10^6 BTU)	AUX (10^6 BTU)	Solar (MJ)	DWH (MJ)	AUX (MJ)	f
Jan	0.585	1.14	0.902	617.2101	1202.768	951.6641	0.209
Feb	0.642	1.027	0.75	677.3485	1083.547	791.295	0.27
Mar	0.827	1.132	0.765	872.5346	1194.328	807.1209	0.324
Apr	0.929	1.089	0.664	980.1507	1148.96	700.5598	0.39
May	0.976	1.118	0.663	1029.739	1179.557	699.5048	0.407
Jun	0.932	1.076	0.637	983.3159	1135.245	672.0732	0.408
Jul	0.89	1.107	0.682	939.0034	1167.951	719.5509	0.384
Aug	0.891	1.108	0.685	940.0585	1169.006	722.7161	0.382
Sep	0.855	1.076	0.674	902.0763	1135.245	711.1104	0.374
Oct	0.796	1.122	0.757	839.8278	1183.777	798.6804	0.325
Nov	0.627	1.095	0.825	661.5226	1155.291	870.4245	0.247
Dec	0.548	1.138	0.92	578.1729	1200.658	970.6552	0.192
Year	9.499	13.229	8.924	10022.01	13957.39	9415.355	0.326

The values of Table 3 and 4 give an average f value of 24.3%, and 32.5%, for SRCC and CPP data respectively. These values are are both on the low end for typical solar thermal applicatons. For comparison, an *f*-chart analysis using 50 gallons (189.3 L) of storage and a SUNEARTH TRB-40 collector using the same parameters as those that were used for the Copperheart ICS f-chart simulations was carried out resulting in an annual average f = 68%. The SUNEARTH TRB-40 collector system is slightly more complex than the Copperheart ICS. The SRCC data approximates a linear curve for the ICS in order to analyze it as a standard flat plate collector in lieu of an ICS. Consequently, the performance curve considers the fact that the stored water is exposed overnight, lowering the performance dramatically. The Copperheart ICS is better suited for situations where the demand more closely matches the supply. If hot water usage occurs before days end, the f-factor may be closer to the value calculated using a traditional active loop/collector system. Figure 12 shows a bar-chart comparsion of the f-chart output for the SRCC and the CPP data, respectively.

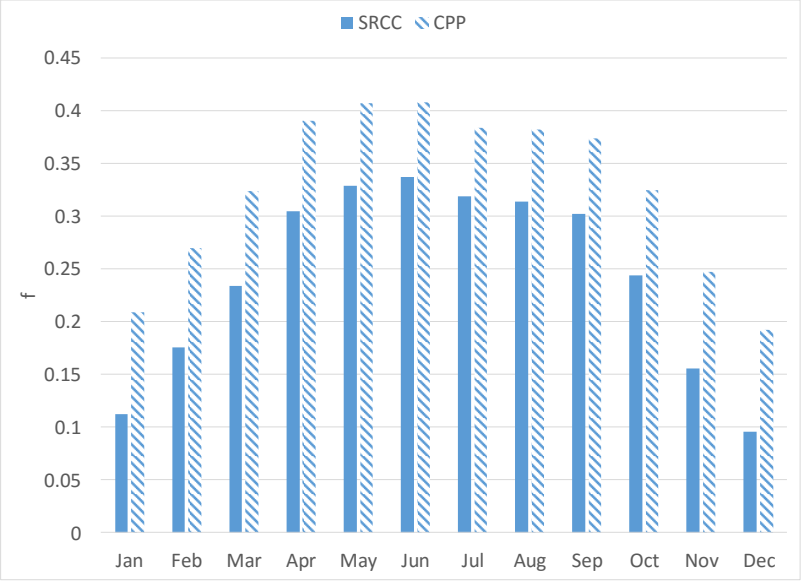

Fig. 12: F-chart output bar-chart comparison between SRCC and CPP inputs

As shown in Figure 12, the CPP f-chart predictions are on average a value of $\Delta f = 0.1$ larger than the SRCC values for each month of the simulation. This is due to the input value of the test slope and test intercept of the CPP data into the f-chart program.

2.4. Transient Modelling

Transient system modelling for the ICS was carried out per the following expression (Goswami et al. 2000)

$$\tau = \frac{C_{plate} + U_c / U_\infty C_{glass}}{U_c A}$$

$$C = mc_p \qquad \text{(eq. 15)}$$

$$T_p = T_\infty + \frac{\alpha_s I_s}{U_c} - \left[\frac{\alpha_s I_s}{U_c} - (T_{p,o} - T_a)\right]\exp(-t/\tau)$$

Figure 13 shows a typical transient output using the model of eq. 15 corresponding to the environmental loading data of Table 5.

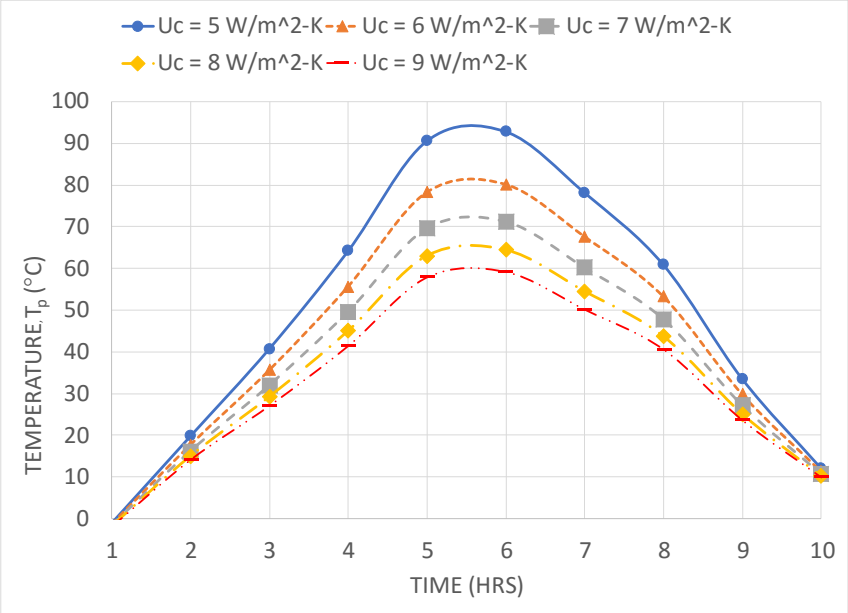

Fig. 13: Transient Model Simulation Results

Tab. 5 Environmental Loading for Transient Simulation

Time (hr)	I_s (W/m^2)	T_a (K)
7-8	12	270
8-9	80	280
9-10	192	283
10-11	320	286
11-12	460	290
12-13	474	290
13-14	395	288
14-15	287	288
15-16	141	284
16-17	32	280

As expected the transient modeling output of Figure 13 displays the time lag associated with the ICS when being forced by different values of convection loss U_c = 5, 6, 7, 8, 9 W/m^2-K, respectively.

3. Conclusions

This paper has presented the results of an experimental study and thermal modeling of an ICS solar thermal apparatus. The concept of the ICS was reviewed, followed by an explanation of a test apparatus and corresponding results for the efficiency performance curve of the ICS. If was found that under actual testing conditions, the slope and intercept data was in slight disagreement with published values for the ICS apparatus. The differences in actual test slope and intercept to previously published values is attributable to actual installation effects, i.e. tree shading, and instrumentation mounting errors, i.e. thermocouple compensation needed since actual thermocouples were not mounted directly on the collector tubes of the ICS, instead they were mounted on the collector glass surface and on the inlet and outlet tubes of the ICS. Nevertheless, the slope intercept data taken indicate an average efficiency on the order of 65% for the ICS. Thermal modeling using the f-chart method indicates that the performance of the ICS affords a solar fraction of f = 33%, which is for a small bungalow located in the Southwest region of the USA. The paper concludes with a transient time based analysis of the ICS for particular loading profile with indicates the effect of the top loss coefficient due to local wind speed. The transient simulations indicate that the peak temperature of the ICS is attenuated from 35 °C over the range of $5 < U < 9$ W/m^2-K. Thus, the energy storage capability of the ICS is profoundly influenced by the local wind speed value.

4. References

Goswami, D. Y., Kreith, F., and Krieder, J.F., 2000. Principles of Solar Engineering, second ed., Taylor and Francis, New York.

Kalogirou, S.A. 1999. Performance enhancement of an integrated collector storage hot water system. Renewable Energy, Vol. 16, Issue 1, pp. 652-655.

Kalogirou, S.A., 2009. Solar Energy Engineering: Processes and Systems, Academic Press, Massachusetts.

Klein, S.A. and Duffie, W.A. , 2008. F-Chart Active and Passive Solar Systems Analysis.

Klein, S.A., Beckman, W.A., and Duffie, J.A., 1976. A Design Procedure For Solar Heating Systems, Solar Energy, Vol. 18, pp. 113- 126.

Kocaa, A., Oztopb, H., Koyunc, T., and Varol, Y., 2008. Energy and exergy analysis of a latent heat storage system with phase change material for a solar collector, Renewable Energy, Vol. 33, Issue 4, pp. 567-574.

Smyth, M., Eames, P.C., and Norton, B., 2004. Integrated collector storage solar water heaters. Renewable and Sustainable Energy Reviews, Vol. 10, pp. 503-538.

Struckmann, F., 2008. Analysis of a Flat-Plate Solar Collector,Heat and Mass Transport, May 8, Lund, Sweden.

Tsilingiris, P.T., 1996. Design and performance of large low-cost solar water heating systems. Renewable Energy, Vol. 9, Issues 1-4, pp. 617-621.

Appendix: **UNITS AND SYMBOLS IN SOLAR ENERGY**

In 1977, a committee of ISES developed a set of recommended nomenclature for papers appearing in *Solar Energy*. This is a condensed and revised version of those recommendations. The original appeared in *Solar Energy* **21**.61-68 (1978).

1. UNITS

The use of S.I. (Système International d'unités) in *Solar Energy* papers is mandatory. The following is a discussion of the various S.I. units relevant to solar energy applications.

Energy
The S.I. unit is the joule (J ≡ kg m^2 s^{-2}). The calorie and derivatives, such as the langley (cal cm^{-2}), are not acceptable. No distinction is made between different forms of energy in the S.I. system so that mechanical, electrical and heat energy are all measured in joules. Because the watt-hour is used in many countries for commercial metering of electrical energy, its use is tolerated here as well.

Power
The S.I. unit is the watt (W ≡ kg m^2 s^{-3} ≡ J s^{-1}). The watt will be used to measure power or energy rate for all forms of energy and should be used wherever instantaneous values of energy flow rate are involved. Thus, energy flux density will be expressed as W m^{-2} and heat transfer coefficient as W m^{-2} K^{-1}. Energy rate should not be expressed as J h^{-1}.
When power is integrated for a time period, the result is energy that should be expressed in joules, e.g. an energy rate of 1.2 kW would produce 1.2 kW x 3600 s = 4.3 MJ if maintained for 1 h. It is preferable to say that

Hourly energy = 4.3 MJ

rather than

Energy=4.3 MJ h^{-1}.

Force
The S.I. unit is the Newton (N ≡ kg m s^{-2}). The kilogram weight is not acceptable.

Pressure
The S.I. unit is the Pascal (Pa ≡ N m^{-2} ≡ k^2 m^{-1} s^{-2}). The unit kg cm^{-2} should not be used. It is sometimes practical to use 10^5 Pa = 1 bar = 0.1 MPa. The atmosphere (1 atm = 101.325 kPa) and the bar, if used, should be in parenthesis, after the unit has been first expressed in Pascals. e.g. 1.23 x 10^6 Pa (12.3 atm). Manometric pressures in meters or millimeters are acceptable if one is reporting raw experimental results. Otherwise they should be convened to Pa.

Velocity
Velocity is measured in m s^{-1}. Popular units such as km h^{-1} may be in parentheses afterward.

Volume
Volumes are measured in m^3 or litres (1 litre = 10^{-3} m^3). Abbreviations should not be used for the litre.

Flow
In S.I. units, flow should be expressed in kg s^{-1}, m^3 s^{-1}, litre s^{-1}. If non-standard units such as litre min^{-1} or kg h^{-1} must be used, they should be in parentheses afterward.

Temperature
The S.I. unit is the degree Kelvin (K). However, it is also permissible to express temperatures in the degree Celsius (°C). Temperature differences are best expressed in Kelvin (K).
When compound units involving temperature are used, they should be expressed in terms of Kelvin, e.g. specific heat J kg^{-1} K^{-1}.

2. NOMENCLATURE AND SYMBOLS

Tables 1-5 list recommended symbols for physical quantities. Obviously, historical usage is of considerable importance in the choice of names and symbols and attempts have been made to reflect this fact in the tables. But conflicts do arise between lists that are derived from different disciplines. Generally, a firm recommendation has been made for each quantity, except for radiation where two options are given in Table 5.
In the recommendations for *material properties* (see Table 1), the emission, absorption, reflection, and transmission of radiation by materials have been described in terms of quantities with suffixes 'ance' rather than 'ivity', which is also sometimes used, depending on the discipline. It is recommended that the suffix 'ance' be used for the following four quantities:

$$\text{emittance } \varepsilon = \frac{E}{E_b}\left(or \frac{M_s}{M_{sb}} \right)$$

$$\text{absorptance } \alpha = \frac{\Phi}{\Phi_i}$$

$$\text{reflectance } \rho = \frac{\Phi}{\Phi_i}$$

$$\text{transmittance } \tau = \frac{\Phi}{\Phi_i}$$

where E and ϕ is the radiant flux density that is involved in the particular process. The double use of α for both absorptance and thermal diffusivity is usual, as is the double use of ρ for both reflectance and density. Neither double use should give much concern in practice.

Table 1: Recommended symbols for materials properties

Quantity	Symbol	Unit
Specific heat	c	J kg^{-1} K^{-1}
Thermal conductivity	k	W m^{-1} K^{-1}
Extinction coefficient[+]	K	m^{-1}
Index of refraction	n	
Absorptance	α	
Thermal diffusivity	α	m^2 s^{-1}
Specific heat ratio	γ	
Emittance	ε	
Reflectance	ρ	
Density	ρ	kg m^{-3}
Transmittance	τ	

[+] In meteorology, the *extinction coefficient* is the product of K and the path length and is thus dimensionless.

Table 2: Recommended symbols and sign convention for sun and related angles

Quantity	Symbol	Range and sign convention
Altitude	α	0 to ± 90°
Surface tilt	β	0 to ± 90°; toward the equator is +ive
Azimuth (of surface)	γ	0 to 360°; clockwise from North is +ive
Declination	δ	0 to ± 23.45°
Incidence (on surface)	Θ,i	0 to + 90°
Zenith angle	Θ_z	0 to + 90°
Latitude	Φ	0 to ± 90°; North is +ive
Hour angle	ω	-180° to +180°; solar noon is 0°, afternoon is +ive
Reflection (from surface)	r	0 to + 90°

Table 3: Recommended symbols for miscellaneous quantities

Quantity	Symbol	Unit
Area	A	m^2
Heat transfer coefficient	h	W m^{-2} K^{-1}
System mass	m	kg
Air mass (or air mass factor)	M	
Mass flow rate	$\dot{m}$	kg s^{-1}
Heat	Q	J
Heat flow rate	$\dot{Q}$	W
Heat flux	q	W m^{-2}
Temperature	T	K
Overall heat transfer coefficient	U	W m^{-2} K^{-1}
Efficiency	η	
Wavelength	λ	m
Frequency	ν	s^{-1}
Stefan-Boltzmann constant	σ	W m^{-2} K^{-4}
Time	t,τ,Θ	s

Table 4: Recommended subscripts

Quantity	Symbol
Ambient	a
Black-body	b
Beam (direct)	b
Diffuse (scattered)	d
Horizontal	h
Incident	i
Normal	n
Outside atmosphere	o
Reflected	r
Solar	s
Solar constant	sc
Sunrise (sunset)	sr, (ss)
Total of global	t
Thermal	t, th
Useful	u
Spectral	λ

Table 5: Recommended symbols for radiation quantities

	Preferred name	Symbol	Unit
a)	Nonsolar radiation		
	Radiant energy	Q	J
	Radiant flux	Φ	W
	Radiant flux density	Φ	W m^{-2}
	Irradiance	E, H	W m^{-2}
	Radiosity or Radiant exitance	M, J	W m^{-2}
	Radiant emissive power (radiant self-exitance)	Ms, E	W m^{-2}
	Radiant intensity (radiance)	L	W m^{-2} sr^{-1}
	Irradiation or radiant exposure	H	J m^{-2}
b)	Solar radiation		
	Global irradiance or solar flux density	G	W m^{-2}
	Beam irradiance	G_b	W m^{-2}
	Diffuse irradiance	G_d	W m^{-2}
	Global irradiation	H	J m^{-2}
	Beam irradiation	H_b	J m^{-2}
	Diffuse irradiation	H_d	J m^{-2}
c)	Atmospheric radiation		
	Irradiation	$\Phi\downarrow$	W m^{-2}
	Radiosity	$\Phi\uparrow$	W m^{-2}
	Exchange	Φ_N	W m^{-2}